**International Journal of Recent Innovations in Academic Research**

E-ISSN: 2635-3040; P-ISSN: 2659-1561
Homepage: https://www.ijriar.com/
Volume-10, Issue-1, January-March-2026: 86-104

**Research Article**

# Green-Synthesized Cobalt-Doped Magnesium Oxide Nanoparticles for Efficient Removal of Brilliant Green Dye: Adsorption Study and Process Optimization Using Response Surface Methodology

**[*a]Andriamampandry Mazoa Methode, [b]Ch. Asha Immanuel Raju, [c]Heriniaina Ny Hafaliana Koloina, [d]Tamirat Lamaro Bate and [e]Randrianoelivony Andriniaina Mahefa**

[a-e]Department of Chemical Engineering, College of Engineering, Andhra University, Visakhapatnam-530 003, Andhra Pradesh, India
*Corresponding Author Email: mazoandriam10@gmail.com

**Article History**
**Received:** January 30, 2026
**Accepted:** February 23, 2026
**Published:** March 02, 2026

**Abstract**
Cobalt-doped magnesium oxide nanoparticles (Co-MgO NPs) were synthesized via a *Moringa oleifera* leaf-extract–assisted route and evaluated for the removal of Brilliant Green (BG) dye from aqueous solutions. The adsorbent was characterized using SEM, XRD, FTIR, and EDX, confirming MgO formation with cobalt incorporation and a nanoscale morphology (≈ 82 nm from SEM). Batch adsorption experiments were conducted to examine the effects of contact time, initial BG concentration, solution pH, adsorbent dosage, and temperature. Process optimization was carried out using response surface methodology (RSM). Under the optimized conditions (contact time ≈ 100 min, $C_0$ = 20 mg/L, pH = 6, dosage = 3 g/L, and T = 303 K), a maximum BG removal efficiency of 92.1% was obtained. Equilibrium data were best described by the Freundlich model ($R^2$ = 0.998), and the pseudo-second-order kinetic model provided the best fit among the kinetic models ($R^2$ = 0.9994). Thermodynamic parameters indicated a spontaneous and exothermic adsorption process.
**Keywords:** *Moringa oleifera*, Brilliant Green Dye, Co–MgO Nanoparticles, Adsorption Isotherms, Kinetics, Thermodynamics, Response Surface Methodology (RSM).

## 1. Introduction

Freshwater availability is increasingly constrained by population growth, rapid urbanization, and expanding industrial activity. At the same time, the discharge of inadequately treated effluents continues to degrade natural water bodies, making dye-containing wastewater a persistent concern in many regions [1–3]. Industrial effluents from textile, paper, leather, printing, and dyeing operations often contain synthetic colorants and auxiliary chemicals that are resistant to conventional treatment. Even at low concentrations, dyes reduce light penetration, disrupt photosynthetic activity, and may harm aquatic life [4–6].

Brilliant Green (BG) is a cationic triphenylmethane dye widely used for textile dyeing, paper printing, and biological staining. BG is associated with toxicity and potential mutagenic effects, and its persistence in the aquatic environment raises serious health and ecological concerns [4,8]. Conventional wastewater treatment methods such as coagulation–flocculation, membrane filtration, and biological degradation can suffer from high operating costs, incomplete color removal, sludge generation, and sensitivity to operating conditions [5,7,9].

Adsorption is attractive for dye removal because it is simple to operate and can achieve high removal efficiency across a wide range of conditions. Nanostructured adsorbents are particularly promising due to their high surface area and tunable surface chemistry [6,10]. Magnesium oxide (MgO) is chemically stable and non-toxic, and it exhibits affinity toward organic pollutants. Moreover, doping MgO with transition metals such as cobalt can modify surface reactivity and defect density, potentially improving adsorption performance [2,11].

In this work, cobalt-doped MgO (Co-MgO) nanoparticles were prepared via a green, plant-assisted route using *Moringa oleifera* leaf extract as a reducing and stabilizing medium. The material was characterized using SEM, XRD, FTIR, and EDX. Batch experiments were performed to study the effects of contact time, initial dye concentration, pH, adsorbent dosage, and temperature on BG removal. Response surface methodology (RSM) was then applied to optimize the operating conditions and to evaluate interaction effects. Equilibrium, kinetic, and thermodynamic analyses were used to describe the adsorption behavior and to provide mechanistic insight.

## 2. Experimental Procedures

### 2.1 Materials

Magnesium nitrate hexahydrate ($Mg(NO_3)_2{\cdot}6H_2O$), cobalt nitrate hexahydrate ($Co(NO_3)_2{\cdot}6H_2O$), sodium hydroxide (NaOH), and Brilliant Green dye were of analytical grade and used as received. Fresh *Moringa oleifera* leaves were collected locally for extract preparation. Distilled water was used for all solution preparations.

### 2.2 Preparation of Moringa Leaf Extract

Fresh *Moringa oleifera* leaves were washed thoroughly with distilled water to remove dust and surface impurities and then finely chopped. Approximately 20 g of leaves were added to 100 mL of distilled water and heated at 80 °C for 30 min under continuous stirring. The mixture was cooled to room temperature and filtered through Whatman filter paper to obtain a clear extract, which was used immediately as a reducing and stabilizing agent.

### 2.3 Green Synthesis of Cobalt-Doped Magnesium Oxide Nanoparticles

Magnesium nitrate hexahydrate (1.153 g) and cobalt nitrate hexahydrate (0.145 g) were dissolved separately in 100 mL of distilled water. The two solutions were mixed at ambient temperature, and NaOH (4 g) was added gradually under stirring (15 min) to initiate precipitation. Subsequently, 20 mL of *Moringa* leaf extract was added slowly, and the mixture was stirred at 70 °C for 3 h. The resulting paste was dried in a hot-air oven at 100 °C for 2 h and then calcined in a muffle furnace at 500 °C for 3 h to obtain Co–MgO nanoparticles. Based on the precursor ratio, the target Co/(Co + Mg) molar fraction was approximately 0.10.

### 2.4 Preparation of Brilliant Green Dye Stock Solution

A stock solution of Brilliant Green dye (1000 mg/L) was prepared by dissolving 1 g of dye in 1 L of distilled water. Working solutions (10–50 mg/L) were prepared by appropriate dilution of the stock solution using distilled water.

### 2.5 Characterization of Synthesized Nanoparticles

The surface morphology of the synthesized Co–MgO nanoparticles was characterized using scanning electron microscopy (SEM). The structural and morphological properties were examined using X-ray diffraction (XRD) to determine crystallinity and phase composition, while functional groups and surface interaction were identified using Fourier transform infrared spectroscopy (FTIR). In addition, the elemental composition was analyzed by energy-dispersive X-ray spectroscopy (EDX).

### 2.6 Batch Adsorption Experiments

Batch adsorption experiments were conducted to evaluate Brilliant Green removal using Co–MgO nanoparticles. A measured dose of adsorbent was added to a fixed volume of dye solution of known initial concentration and agitated at a constant speed. Aliquots were collected at predetermined time intervals, and the residual dye concentration was measured using a UV–visible spectrophotometer at the maximum absorbance wavelength ($\lambda_{max}$) of BG.

Removal efficiency was calculated as:

$$\text{Removal (\%)} = ((C_0 - C_t) / C_0) \times 100,$$

Where,

$C_0$ and $C_t$ (mg/L) are the initial and residual dye concentrations at time t, respectively. The adsorption capacity at equilibrium ($q_e$, mg/g) was calculated using:

$$q_e = (C_0 - C_e)V / m,$$

Where,

$C_e$ (mg/L) is the equilibrium concentration, V (L) is the solution volume, and m (g) is the mass of adsorbent.

**Table 1.** Experimental conditions investigated for BG adsorption.

| S/N | Parameters | Values investigated |
|---|---|---|
| 1 | Contact time (min) | 5, 10, 20, 30, 40, 50, 60, 80, 100, 120, 150, and 180 |
| 2 | Initial dye concentration (mg/L) | 10, 20, 30, 40, and 50 |
| 3 | pH of aqueous solution | 3, 4, 5, 6, 7, 8, 9, and 10 |
| 4 | Adsorbent dosage (g/L) | 0.5, 1, 1.5, 2, 2.5, and 3 |
| 5 | Temperature (K) | 303, 313, 323, 333, and 343 |

### 2.7 Adsorption Isotherms, Kinetics, and Thermodynamic Studies

Adsorption isotherms, including Langmuir, Freundlich, and Temkin isotherms, were applied to analyze the equilibrium adsorption behavior. Kinetic models such as pseudo-first-order and pseudo-second-order were used to evaluate the adsorption rate mechanism. Thermodynamic parameters, including Gibbs free energy (ΔG°), enthalpy (ΔH°), and entropy (ΔS°), were determined to assess the feasibility and nature of the adsorption process.

### 2.8 Response Surface Methodology (RSM)

Response surface methodology was employed to optimize the adsorption process parameters and to evaluate interaction effects on BG removal. A central composite design was used, and statistical analysis was performed to determine the optimal operating conditions for maximum Brilliant Green removal.

## 3. Results and Discussion

### 3.1 Characterization Studies

#### 3.1.1 SEM Analysis

The surface morphology of the synthesized Co–MgO was examined by SEM (Figure 1). The images show rod-like and plate-like nanostructures with irregular sizes and some degree of agglomeration. From the micrographs, the characteristic particle dimension was in the nanoscale range (≈ 82 nm, estimated from SEM). Such anisotropic features are commonly observed in plant-mediated syntheses, where phytochemicals can preferentially bind to specific crystal facets and influence growth [13,14].

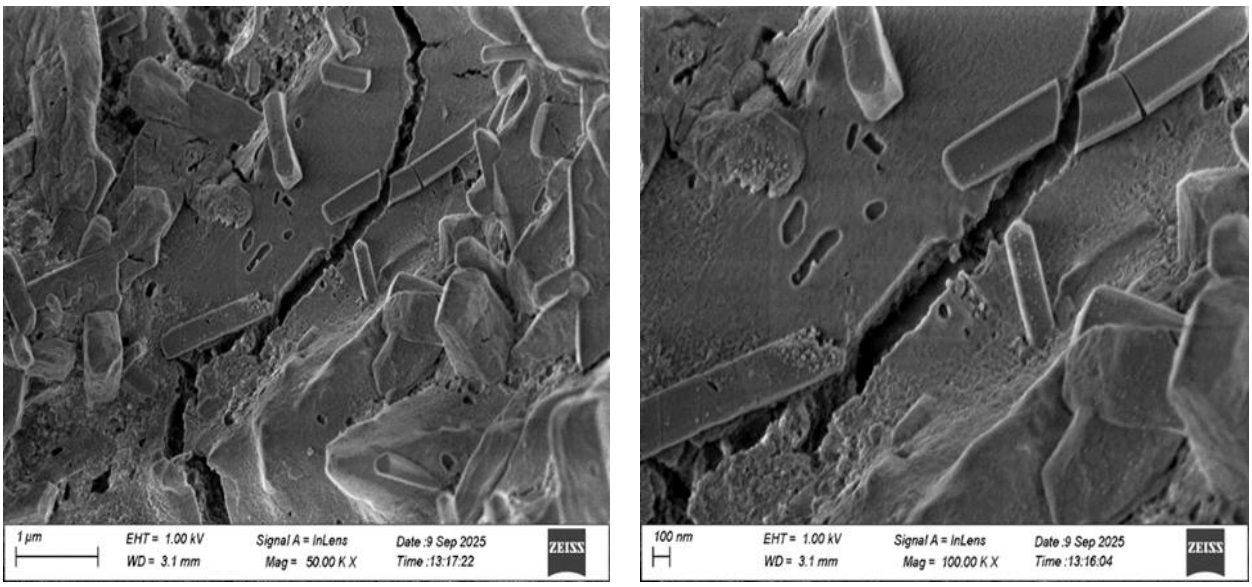


**Figure 1.** SEM micrographs of Co-MgO nanoparticles.

#### 3.1.2 XRD Analysis

Figure 2 shows the XRD pattern of the synthesized Co–MgO nanoparticles. The diffraction peaks at 2θ = 36.9°, 42.9°, 62.3°, and 74.7° correspond to the (111), (200), (220), and (311) planes of cubic MgO, confirming a crystalline MgO phase [15,17]. No additional crystalline phases were observed within the detection limit, suggesting that cobalt was incorporated into the MgO lattice or present in an XRD-amorphous form. The average crystallite size estimated from the Debye–Scherrer equation was approximately 137 nm; this value

should be treated as an approximation because peak broadening can also be influenced by strain and instrumental effects [18]. Differences between SEM-based particle dimensions and Scherrer crystallite sizes can arise from anisotropic morphologies, agglomeration, and the approximate nature of the Scherrer method.

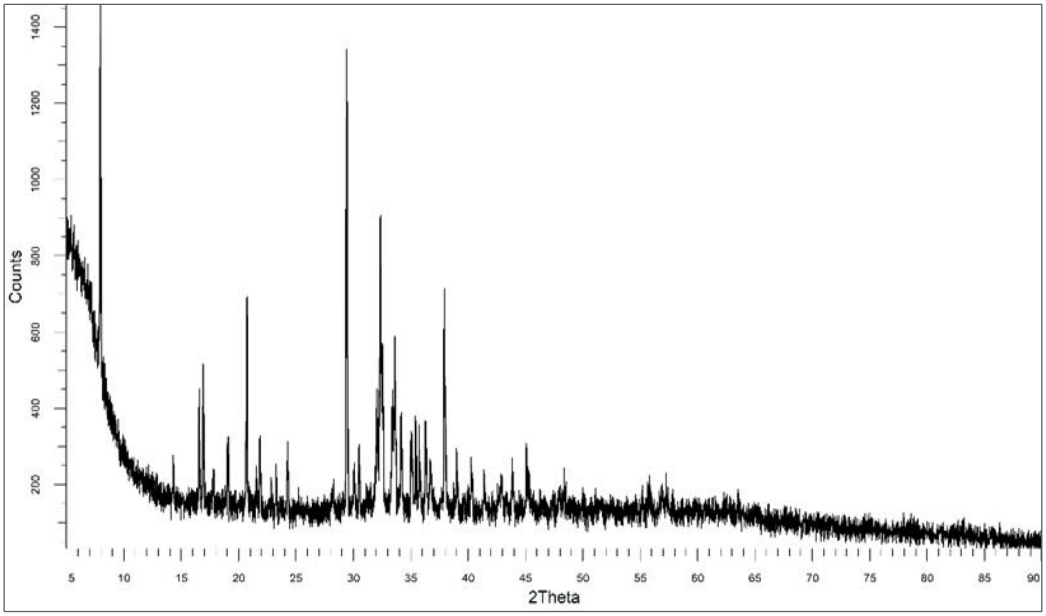


**Figure 2.** XRD pattern of Co-MgO nanoparticles.

### 3.1.3 FTIR Analysis

The FTIR spectrum of the synthesized Co–MgO nanoparticles is shown in Figure 3. The broad band around 3410 $cm^{-1}$ corresponds to O–H stretching of surface hydroxyl groups, while the band near 1645 $cm^{-1}$ is attributed to H–O–H bending of adsorbed water.

Peaks at approximately 1458 and 1385 $cm^{-1}$ can be assigned to carbonate species or residual nitrate from the precursor salts. The characteristic absorption in the 600–400 $cm^{-1}$ region is associated with Mg–O/Co–O lattice vibrations, supporting the formation of cobalt-doped magnesium oxide [14,15,17].

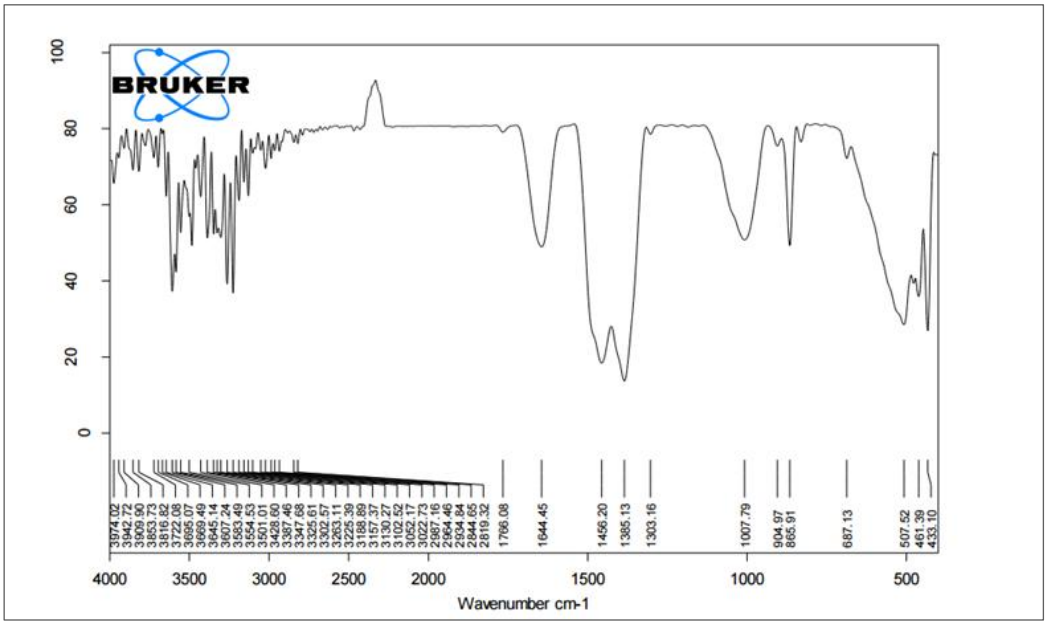


**Figure 3.** FTIR spectrum of Co-MgO nanoparticles.

### 3.1.4 EDX Analysis

EDX analysis (Figure 4) confirmed the presence of magnesium, oxygen, and cobalt in the synthesized material. The detected carbon signal is commonly associated with the carbon tape used for sample mounting or adventitious carbon on the surface. Overall, the spectrum supports cobalt incorporation in the MgO-based adsorbent [16,18].

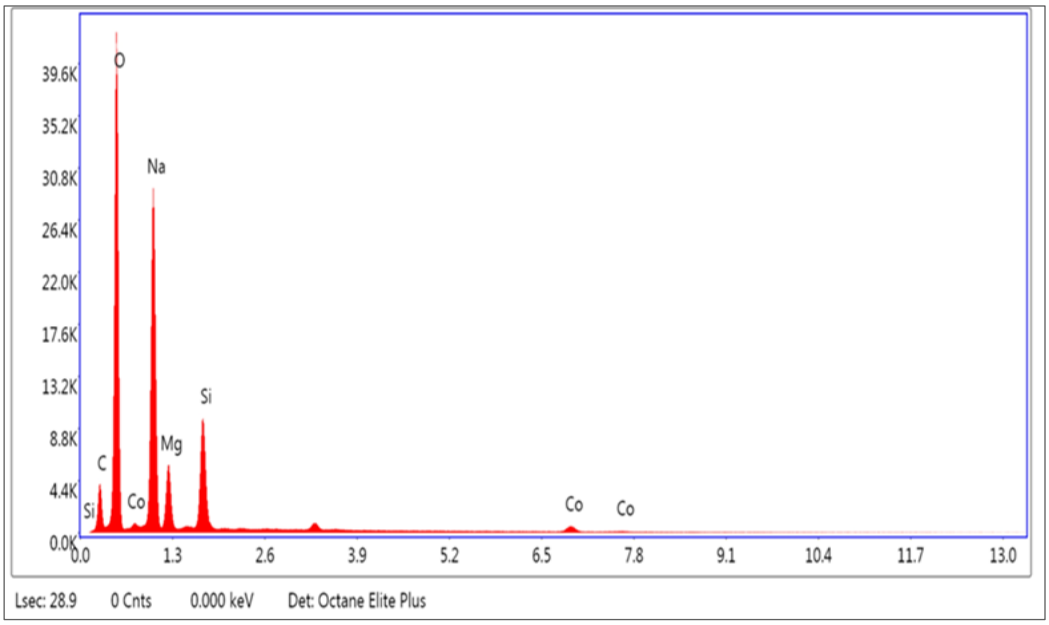


**Figure 4.** EDX spectrum of Co-MgO nanoparticles.

### 3.2 Batch Adsorption Studies

#### 3.2.1 Effect of Contact Time

The effect of contact time (5–180 min) on BG adsorption is shown in Figure 5. The removal efficiency increased rapidly during the initial stage and then gradually approached a plateau, indicating progressive occupation of available active sites. Approximately 69% removal was reached after about 100 min under the conditions used for the time study, and no significant improvement was observed thereafter. Therefore, a contact time of 100 min was selected for subsequent experiments and for RSM optimization [19,21,29,31].

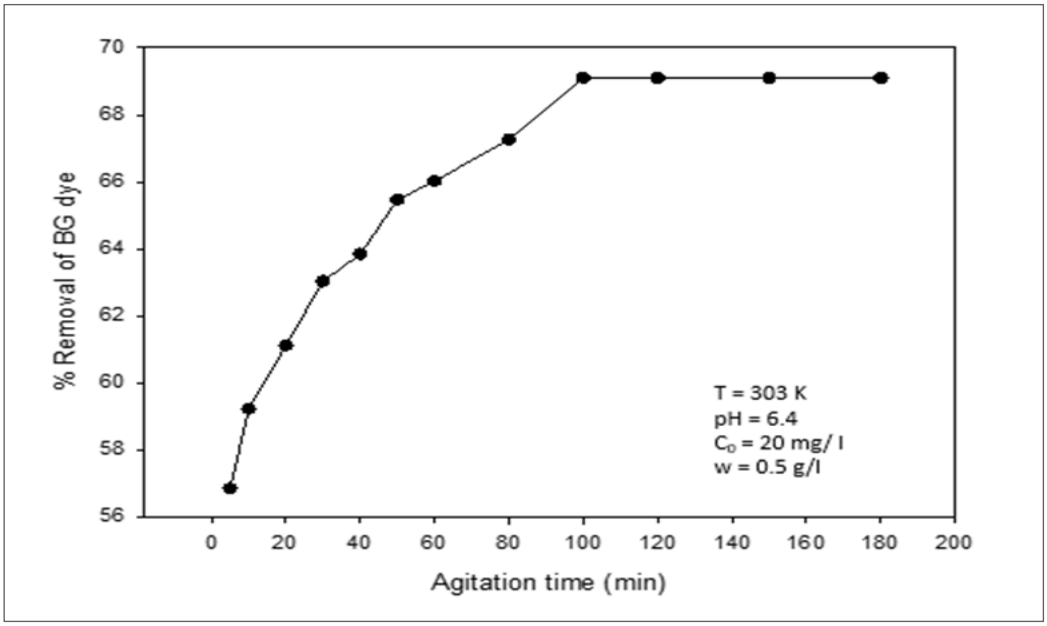


**Figure 5.** Effect of contact time on BG removal (%).

#### 3.2.2 Effect of Initial Concentration of Dye

The influence of initial BG concentration (10–50 mg/L) is shown in Figure 6. As the initial concentration increased, the percentage removal decreased (≈ 84% to ≈ 55%), which can be attributed to the saturation of available adsorption sites at higher solute loading. In contrast, the adsorption capacity (mg/g) increased with concentration because a higher driving force enhances mass transfer of dye molecules from the bulk solution to the adsorbent surface [32–35]. In contrast, the dye uptake (mg/g) shows a continuous increase with increasing initial concentration, as presented in the same figure. Higher concentrations provide a stronger driving force for mass transfer, enabling more dye molecules to accumulate on each gram of the adsorbent despite the reduction in percentage removal [32–35].

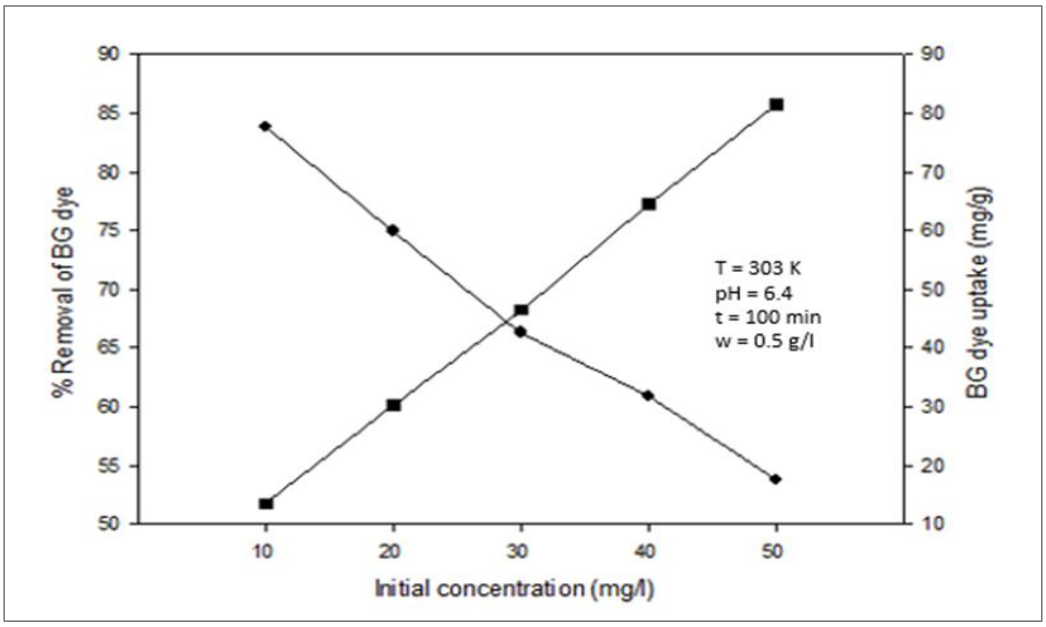


**Figure 6.** Effect of initial BG concentration on removal (%) and adsorption capacity.

### 3.2.3 Effect of pH

The effect of solution pH (3–10) on BG removal is presented in Figure 7. Removal was relatively lower in the acidic range (pH 3–5), which can be associated with protonation of surface functional groups and reduced electrostatic attraction toward the cationic BG molecules. Removal increased to a maximum of about 80% at pH 6, indicating this as an optimum pH under the studied conditions. At higher pH, the removal efficiency declined slightly, which may be related to competition with hydroxide ions and changes in dye speciation or surface charge [36,37]. As the pH increases, the adsorbent surface gradually becomes less protonated and eventually develops a negative charge. This enhances the electrostatic attraction between the negatively charged adsorbent surface and the cationic BG dye molecules. Consequently, the percentage removal increases sharply, reaching a maximum of about 80% at pH 6, indicating this as the optimum pH for BG dye adsorption. Beyond pH 6, the removal efficiency gradually declines, possibly due to competition from excess hydroxide ions or changes in dye solubility under alkaline conditions [36,37].

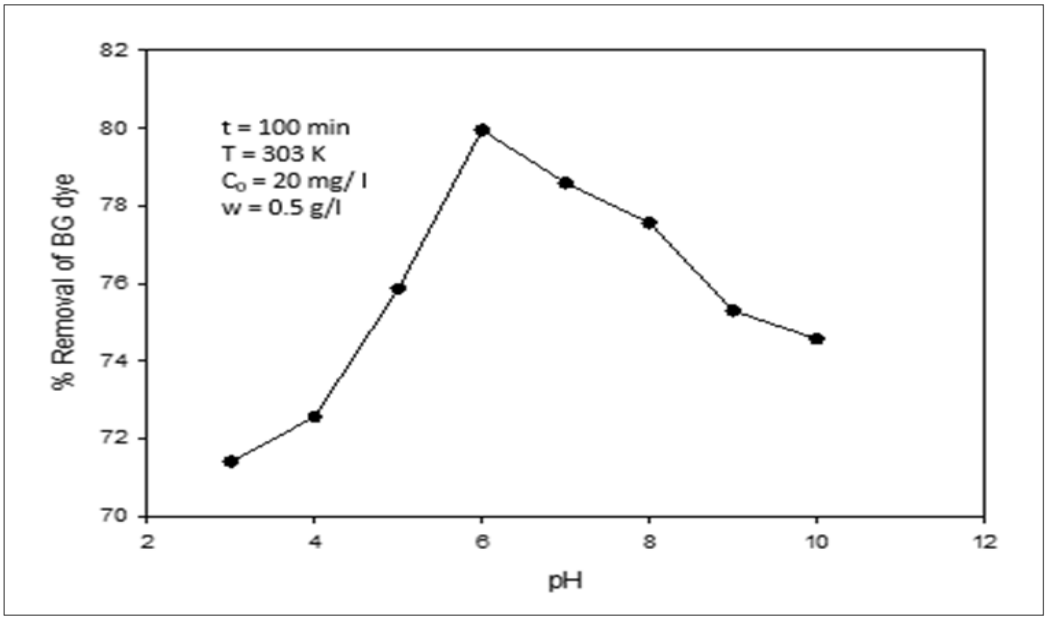


**Figure 7.** Effect of solution pH on BG removal (%).

### 3.2.4 Effect of Co–MgO Nanoparticles Dosage

The influence of adsorbent dosage (0.5–3 g/L) is shown in Figure 8. Increasing the dosage increased BG removal (≈ 75% to ≈ 87%) due to the larger number of available adsorption sites. The improvement became less pronounced at higher dosages, which is typically associated with site overlap/aggregation and a reduced

effective surface area per unit mass. A dosage of 3 g/L was selected as optimum for the subsequent studies and RSM optimization [36–39].

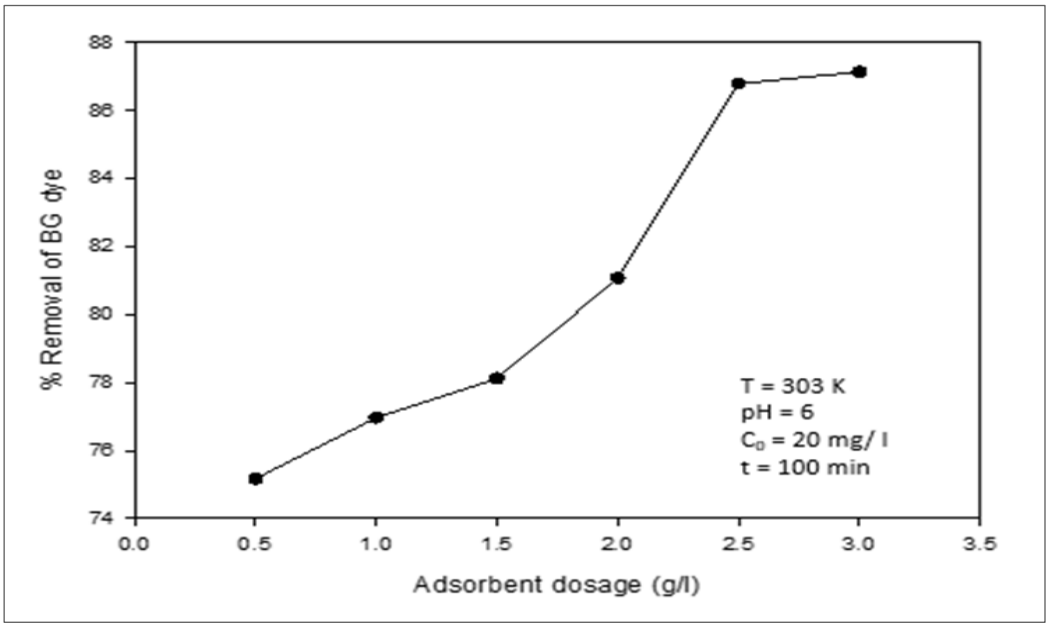


**Figure 8.** Effect of adsorbent dosage on BG removal (%).

### 3.2.5 Effect of Temperature

Figure 9 shows the effect of temperature (303–343 K) on BG adsorption. The removal efficiency decreased slightly with increasing temperature, with a maximum removal of about 92% at 303 K. This trend indicates an exothermic adsorption process, where higher temperatures weaken dye–surface interactions and favor desorption over adsorption [32,33]. Accordingly, 303 K was selected as the optimum temperature for removal.

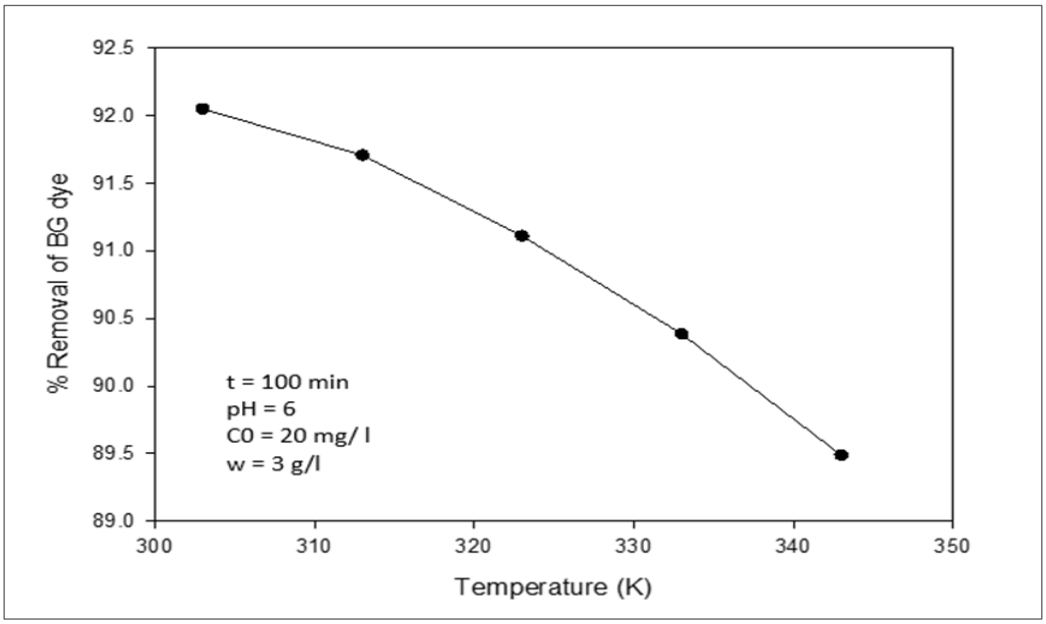


**Figure 9.** Effect of temperature on BG removal (%).

## 3.3 Isotherm Studies

### 3.3.1 Langmuir Isotherm

The Langmuir model assumes monolayer adsorption on a homogeneous surface with a finite number of identical sites [32]. The linearized Langmuir equation is given by:

$$C_e/q_e = (1/(bq_m)) + (C_e/q_m) \ldots (1)$$

A plot of $C_e/q_e$ versus $C_e$ (Figure 10) yielded a straight line ($R^2 = 0.827$). The fitted linear equation was:

$C_e/q_e = 0.0194C_e + 0.03305$ … (2)

From the slope ($1/q_m$) and intercept ($1/(bq_m)$), the Langmuir parameters $q_m$ and b were estimated (Table 2). Using the fitted b value, the dimensionless separation factor $R_l$ was in the range 0.033–0.145 for $C_0$ = 10–50 mg/L ($0 < R_l < 1$), indicating favorable adsorption in the studied concentration range.

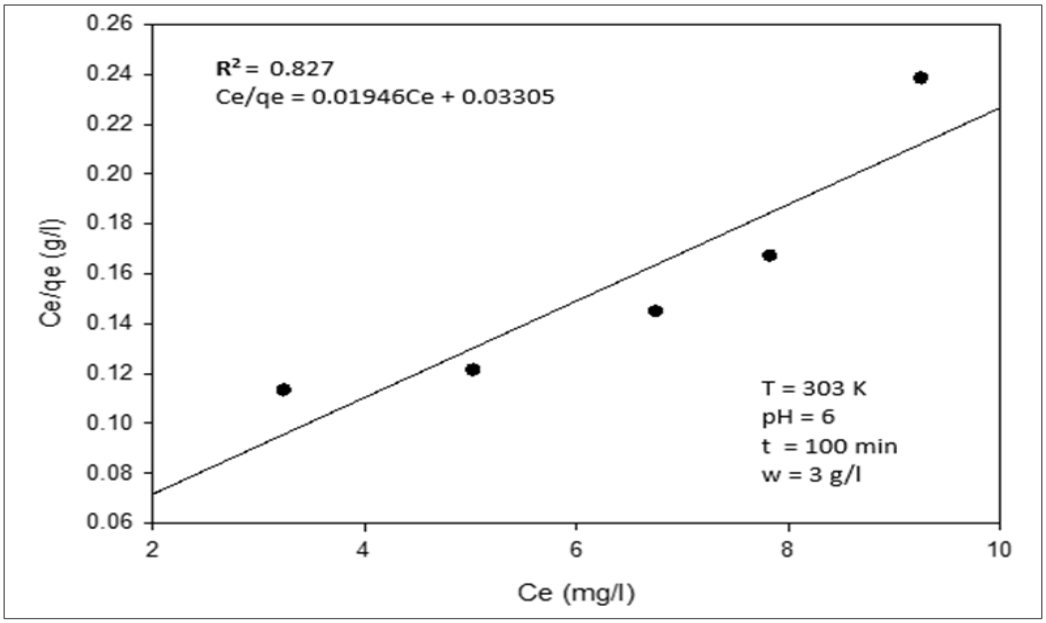


**Figure 10.** Langmuir isotherm plot for BG adsorption.

### 3.3.2 Freundlich Isotherm

The Freundlich model is an empirical isotherm that describes adsorption on heterogeneous surfaces and permits multilayer uptake [33]. Its linear form is:

$\ln(q_e) = \ln(Kf) + (1/n) \ln(C_e)$ … (3)

Figure 11 shows the plot of $\ln(q_e)$ versus $\ln(C_e)$. The slope corresponds to 1/n, and the intercept to ln(Kf). The fitted relation ($R^2$ = 0.9981) was:

$\ln(q_e) = 1.7109 \ln(C_e) + 0.611$ … (4)

The Freundlich constants obtained from the slope and intercept were Kf = 1.84 and $1/n \approx 1.71$ ($n \approx 0.58$) (Table 2). The relatively high 1/n value suggests concentration-dependent uptake and surface heterogeneity.

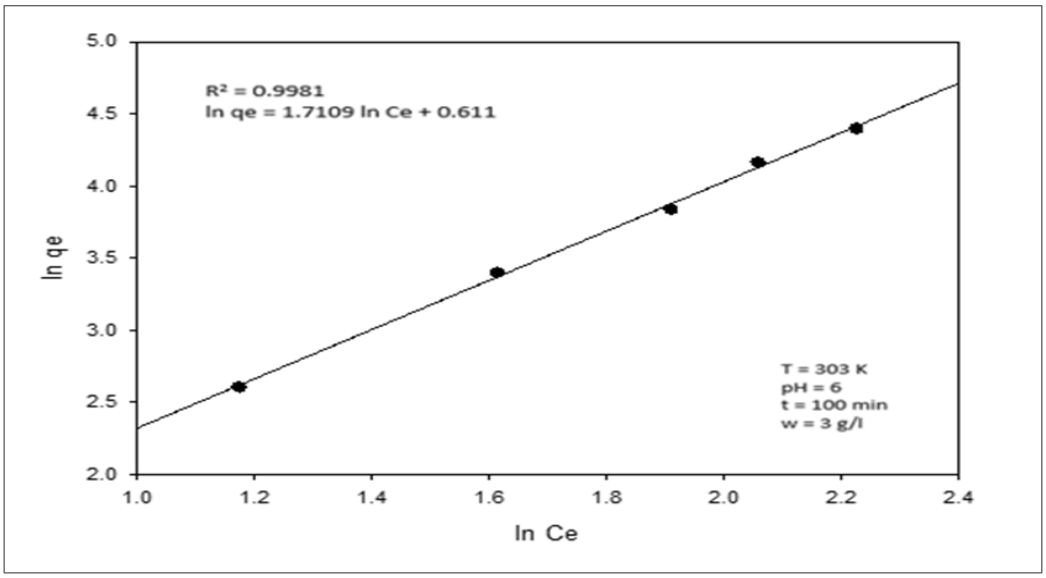


**Figure 11.** Freundlich isotherm plot for BG adsorption.

### 3.3.3 Temkin Isotherm

The Temkin isotherm accounts for adsorbate–adsorbent interactions and assumes that the heat of adsorption decreases linearly with surface coverage [34].

The Temkin equation can be expressed as:

$q_e = (RT/bT) \ln(A_t) + (RT/bT) \ln(C_e)$ … (5)

The plot of $q_e$ versus $\ln(C_e)$ (Figure 12) showed good linearity with $R^2 = 0.973$. Temkin parameters ($A_t$ and bT) were calculated from the intercept and slope, respectively, and are summarized in Table 2.

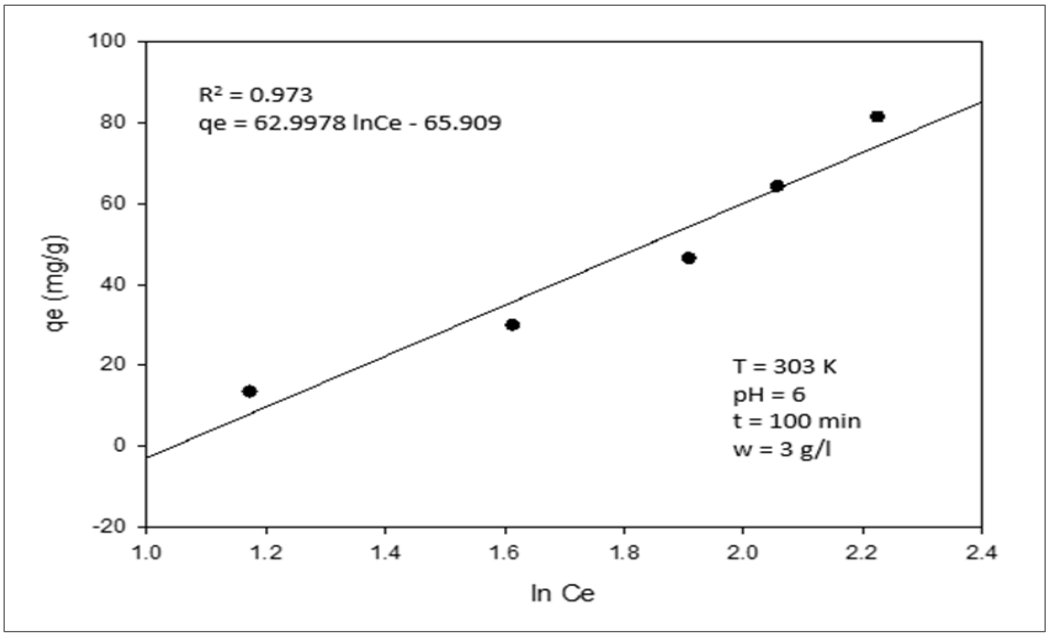


**Figure 12.** Temkin isotherm plot for BG adsorption.

**Table 2.** Isotherm constants obtained for various models.

| Isotherm | Constants | $R^2$ |
|---|---|---|
| Langmuir | qmax (mg/g) = 51.6 | 0.827 |
| | b (L/mg) = 0.589 | |
| | RL ($C_0$ = 10–50 mg/L) = 0.033–0.145 | |
| Freundlich | Kf = 1.84 | 0.998 |
| | n = 0.584 | |
| Temkin | AT = 0.351 | 0.973 |
| | bT = 39.988 | |

Equilibrium data were fitted to the Langmuir, Freundlich, and Temkin models using linear regression of their linearized forms. Among the tested models, the Freundlich isotherm provided the best fit (highest $R^2$), suggesting adsorption on a heterogeneous surface with non-ideal (multilayer) uptake.

Overall, the isotherm analysis indicates that BG adsorption on Co–MgO is better described by a heterogeneous surface model than by an ideal monolayer assumption under the studied conditions.

### 3.4 Kinetics Studies

#### 3.4.1 Pseudo-First-Order Kinetics

Adsorption kinetics were evaluated using pseudo-first-order (Lagergren) and pseudo-second-order models.

The linear pseudo-first-order expression is:

$\log(q_e - q_t) = \log(q_e) - (k_1/2.303)t$ … (6)

A plot of $\log(q_e - q_t)$ versus t (Figure 13) showed good linearity, with $k_1 = 0.02465\ min^{-1}$ and $R^2 = 0.9951$.

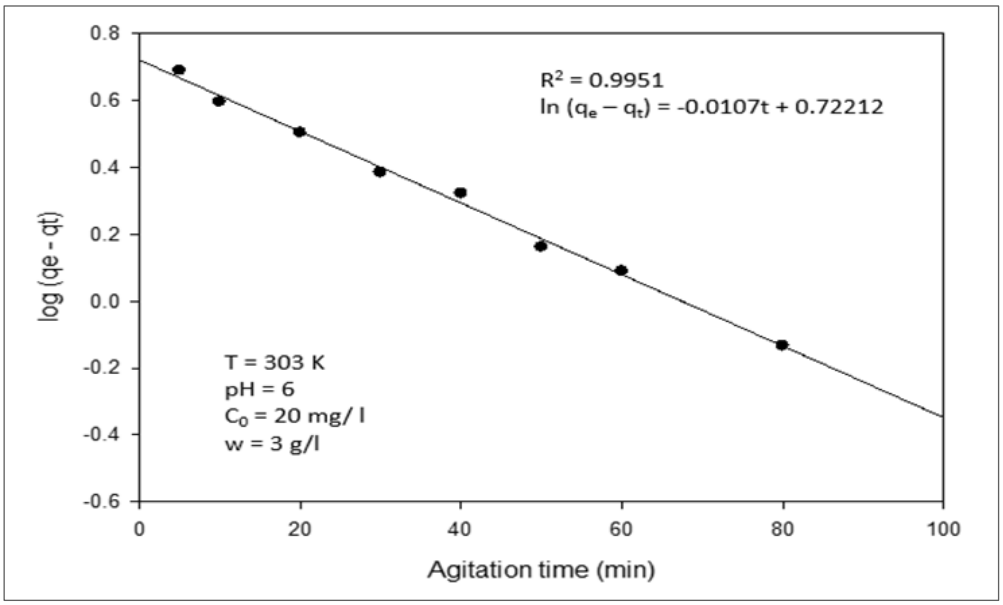


**Figure 13.** Pseudo-first-order kinetic plot for BG adsorption.

### 3.4.2 Pseudo-Second-Order Kinetics

The pseudo-second-order model is frequently used to describe adsorption systems where the overall rate may be governed by surface reactions and/or strong adsorbate–adsorbent interactions [35]. The linearized form is:

$$t/q_t = (1/(k_2 q_e^2)) + (t/q_e) \quad \ldots (7)$$

The plot of $t/q_t$ versus t (Figure 14) provided an excellent fit, with $R^2 = 0.9994$.

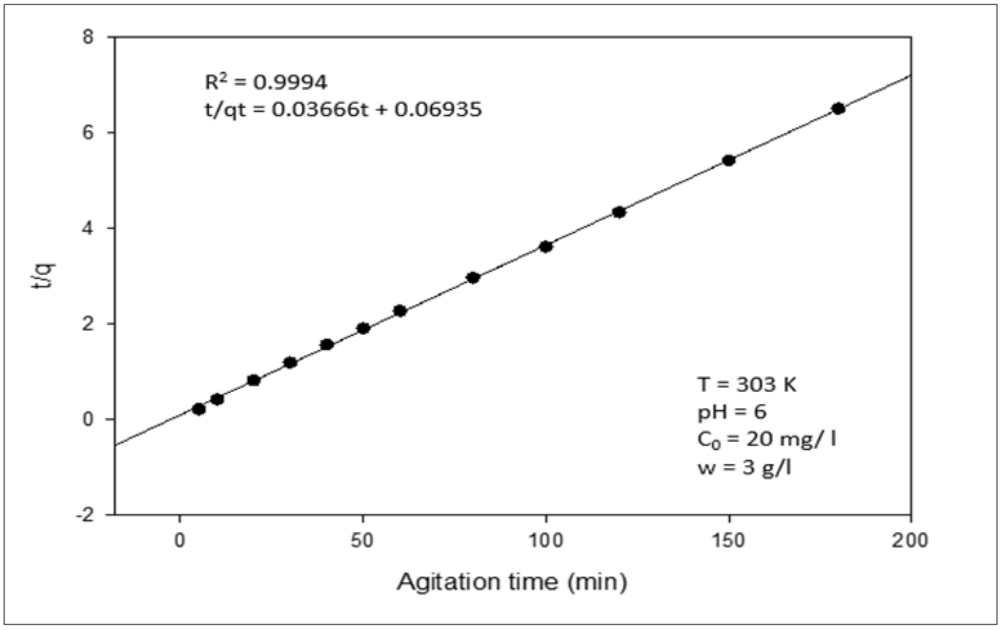


**Figure 14.** Pseudo-second-order kinetic plot for BG adsorption.

**Table 3.** Kinetics data.

| Order | Equation | Rate constant | $R^2$ |
|---|---|---|---|
| Lagergren's first order | $\log (q_e - q_t) = -0.0107t + 0.72212$ | $K_1 = 0.02465\ min^{-1}$ | 0.9951 |
| Pseudo-second order | $t/q_t = 0.03666t + 0.06935$ | $K_2 = 2.8\ g\ mg^{-1}\ min^{-1}$ | 0.9994 |

Both kinetic models provided high correlation coefficients; however, the pseudo-second-order model showed a slightly better fit (higher $R^2$). This indicates that the adsorption rate is well represented by the PSO expression under the studied conditions, although additional transport analysis would be required for a definitive rate-controlling-step assignment.

### 3.5 Thermodynamic Studies

Thermodynamic parameters (ΔH°, ΔS°, and ΔG°) were estimated from temperature-dependent equilibrium data. The Van't Hoff relationship was applied using the apparent equilibrium constant $K_c = q_e/C_e$:

Where,

R is the universal gas constant (8.314 J $mol^{-1}$ $K^{-1}$) and T is the absolute temperature (K).

$$\log(q_e/C_e) = -(\Delta H°/(2.303RT)) + (\Delta S°/(2.303R)) \quad \ldots (8)$$

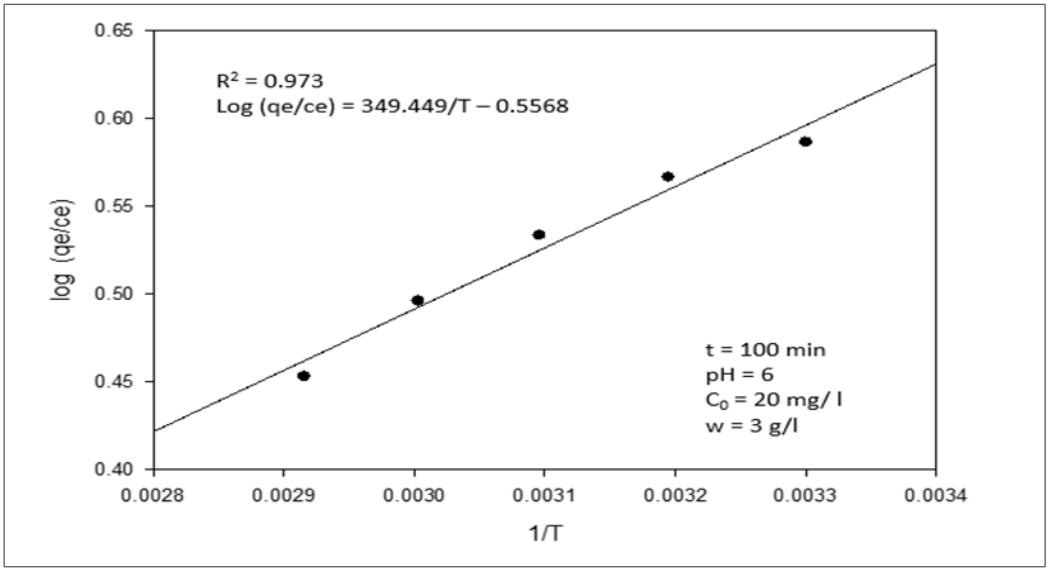


**Figure 15.** Van't Hoff plot for BG adsorption on Co-MgO.

The thermodynamic parameters were obtained from the Van't Hoff plot of $\log(q_e/C_e)$ versus 1/T (Figure 15). The negative enthalpy change (ΔH° = −6690.96 J $mol^{-1}$) indicates an exothermic adsorption process, while the negative entropy change (ΔS° = −10.66 J $mol^{-1}$ $K^{-1}$) suggests decreased randomness at the solid–solution interface. Negative Gibbs free energy values (ΔG° = −3.461 to −3.034 kJ $mol^{-1}$) across the studied temperature range confirm that BG adsorption on Co–MgO is spontaneous under these conditions [37,38].

## 4. Optimization Using Response Surface Methodology (RSM)

### 4.1 Optimization Using Central Composite Design (CCD)

RSM was employed to optimize the operating parameters and to evaluate the combined effects of process variables on BG removal efficiency [40].

The coded levels of the four independent variables used in the CCD are summarized in Table 4.

**Table 4.** Range and levels of parameters.

| Code | Name | Range and levels | | | | |
|---|---|---|---|---|---|---|
| | | **-2** | **-1** | **0** | **1** | **2** |
| $X_1$ | Initial concentration, $C_0$ (mg/L) | 10 | 15 | 20 | 25 | 30 |
| $X_2$ | Dosage, w (g/L) | 2 | 2.5 | 3 | 3.5 | 4 |
| $X_3$ | pH of aqueous solution | 4 | 5 | 6 | 7 | 8 |
| $X_4$ | Temperature, T (K) | 283 | 293 | 303 | 313 | 323 |

In this study, four factors were considered: initial dye concentration ($C_0$, $X_1$), adsorbent dosage (w, $X_2$), solution pH ($X_3$), and temperature (T, $X_4$). Table 5 lists the experimental CCD runs (contact time fixed at 100 min) and the corresponding experimental and model-predicted removal efficiencies.

A second-order polynomial model was fitted to the experimental data to correlate BG removal (%) with the coded variables. The resulting regression equation is:

$$Y = 92.1 - 2.6X_1 + 1.48X_2 + 4.43X_3 - 0.2862X_4 - 0.9008X_1X_2 - 0.30087X_1X_3 - 7.18X_1X_4 - 1.6X_2X_3 - 0.7016X_2X_4 + 6.34X_3X_4 - 1.67X_1^2 - 7.47X_2^2 - 11.95X_3^2 - 5.24X_4^2 \quad \ldots (9)$$

**Table 5.** Results from CCD.

| Run | A: $C_0$ (mg/L) | B: w (g/L) | C: pH | D: T (K) | BG removal (%) | BG removal (%) |
|---|---|---|---|---|---|---|
| | | | | | Experimental | Predicted |
| 1 | 20 | 3 | 6 | 303 | 92.1 | 92.1 |
| 2 | 30 | 3 | 6 | 303 | 86.2 | 80.23 |
| 3 | 10 | 3 | 6 | 303 | 89.2 | 90.62 |
| 4 | 25 | 2.5 | 5 | 293 | 67.8188 | 69.94 |
| 5 | 15 | 3.5 | 5 | 293 | 67.2764 | 67.79 |
| 6 | 15 | 3.5 | 7 | 313 | 85.5201 | 86.39 |
| 7 | 15 | 2.5 | 5 | 313 | 60.3854 | 60.87 |
| 8 | 25 | 3.5 | 7 | 293 | 65.56 | 68.07 |
| 9 | 25 | 3.5 | 5 | 313 | 43.1 | 46.76 |
| 10 | 25 | 2.5 | 5 | 313 | 42.433 | 43.73 |
| 11 | 20 | 3 | 6 | 303 | 92.1 | 92.1 |
| 12 | 20 | 3 | 6 | 303 | 92.1 | 92.1 |
| 13 | 15 | 3.5 | 5 | 313 | 67.8198 | 67.5 |
| 14 | 20 | 4 | 6 | 303 | 67.9476 | 65.2 |
| 15 | 25 | 2.5 | 7 | 293 | 66.9212 | 68.79 |
| 16 | 20 | 2 | 6 | 303 | 61.0726 | 59.28 |
| 17 | 20 | 3 | 4 | 303 | 37.8087 | 35.42 |
| 18 | 20 | 3 | 6 | 283 | 73.5156 | 71.71 |
| 19 | 20 | 3 | 6 | 323 | 73.2962 | 70.56 |
| 20 | 15 | 2.5 | 7 | 293 | 59.0986 | 58.43 |
| 21 | 20 | 3 | 8 | 303 | 55.3115 | 53.15 |
| 22 | 15 | 2.5 | 7 | 313 | 86.0337 | 86.31 |
| 23 | 15 | 3.5 | 7 | 293 | 61.0538 | 61.31 |
| 24 | 25 | 3.5 | 7 | 313 | 63.1302 | 64.41 |
| 25 | 25 | 3.5 | 5 | 293 | 74.5073 | 75.78 |
| 26 | 20 | 3 | 6 | 303 | 92.1 | 92.1 |
| 27 | 20 | 3 | 6 | 303 | 92.1 | 92.1 |
| 28 | 20 | 3 | 6 | 303 | 92.1 | 92.1 |
| 29 | 15 | 2.5 | 5 | 293 | 58.0733 | 58.35 |
| 30 | 25 | 2.5 | 7 | 313 | 65.4583 | 67.93 |

The central composite design comprised 16 factorial points, 8 axial points, and 6 center points (total 30 runs). Contact time was fixed at 100 min during the optimization experiments. ANOVA results for the fitted model are presented in Table 6. In the ANOVA table, factors A–D correspond to $X_1$–$X_4$ (A: concentration, B: dosage, C: pH, and D: temperature). The overall model was significant ($p < 0.0001$). Among the linear terms, A, B, and C were significant ($p < 0.05$), whereas the linear effect of temperature (D) was not significant within the studied range ($p = 0.6126$). The interaction terms AD and CD were significant ($p < 0.0001$), and BC was also significant ($p = 0.0287$), while AB, AC, and BD were not significant at the 95% confidence level.

The coefficient of determination for the model was $R^2 = 0.9900$, indicating that approximately 99.0% of the variation in BG removal was explained by the fitted regression. Center-point replicates showed negligible variation after rounding to one decimal place, which resulted in a near-zero pure error term in the ANOVA table. Based on the ANOVA results, all quadratic terms ($A^2$, $B^2$, $C^2$, and $D^2$) were significant ($p < 0.05$). Significant interactions were observed for AD, BC, and CD, while AB, AC, and BD were not significant within the tested ranges.

Three-dimensional response surface plots (Figure 17 a–f) were generated to visualize the interaction effects between pairs of variables on BG removal. In each plot, two factors were varied while the remaining two were held at their center levels.

For reference, the main-effects (linear) portion of the fitted model can be written as:
$Y = 92.1 - 2.6X_1 + 1.48X_2 + 4.43X_3 - 0.2862X_4$ … (10)

Model adequacy was further assessed by comparing predicted and experimental removal efficiencies (Figure 16).

**Table 6.** ANOVA table for the quadratic model predicting BG removal (%) using CCD.

| Source | Sum of squares | df | Mean square | F-value | p-value | Remark |
|---|---|---|---|---|---|---|
| Model | 7327.48 | 14 | 523.39 | 71.23 | < 0.0001 | Significant |
| A – Conc | 161.89 | 1 | 161.89 | 22.03 | 0.0003 | |
| B – Dosage | 52.50 | 1 | 52.50 | 7.14 | 0.0174 | |
| C – pH | 471.42 | 1 | 471.42 | 64.16 | < 0.0001 | Significant |
| D – Temp | 1.97 | 1 | 1.97 | 0.2675 | 0.6126 | |
| AB | 12.98 | 1 | 12.98 | 1.77 | 0.2036 | |
| AC | 1.53 | 1 | 1.53 | 0.2076 | 0.6552 | |
| AD | 825.74 | 1 | 825.74 | 112.38 | < 0.0001 | Significant |
| BC | 43.04 | 1 | 43.04 | 5.86 | 0.0287 | |
| BD | 7.88 | 1 | 7.88 | 1.07 | 0.3169 | |
| CD | 643.21 | 1 | 643.21 | 87.54 | < 0.0001 | Significant |
| $A^2$ | 76.30 | 1 | 76.30 | 10.38 | 0.0057 | |
| $B^2$ | 1528.63 | 1 | 1528.63 | 208.04 | < 0.0001 | Significant |
| $C^2$ | 3918.73 | 1 | 3918.73 | 533.32 | < 0.0001 | Significant |
| $D^2$ | 753.52 | 1 | 753.52 | 102.55 | < 0.0001 | Significant |
| Residual | 110.22 | 15 | 7.35 | – | – | – |
| Lack of fit | 110.22 | 10 | 11.02 | – | – | – |
| Pure error | 0 | 5 | 0 | – | – | – |
| Cor total | 7437.70 | 29 | – | – | – | – |

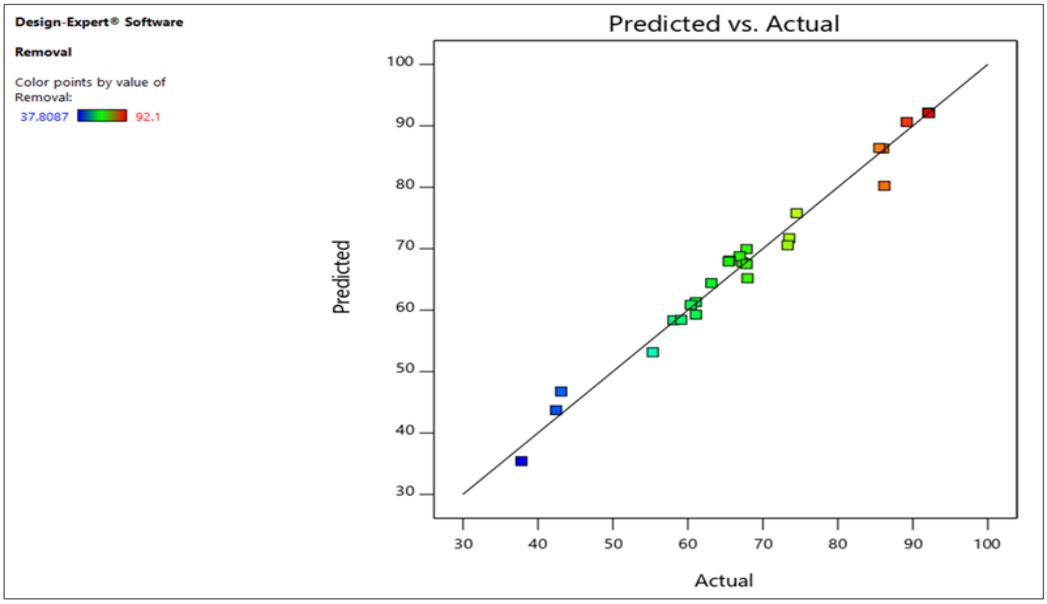


**Figure 16.** Predicted versus experimental BG removal from CCD model.

The optimum operating conditions predicted by the CCD model were validated experimentally (Table 7), showing close agreement between the predicted and observed BG removal.

**Table 7.** Comparison between CCD-predicted optimum conditions and experimental verification.

| Variable | CCD value | Experimental value |
|---|---|---|
| pH of aqueous solution | 5.854 | 6 |
| Initial dye concentration, $C_0$ (mg/L) | 20.708 | 20 |
| Dosage, w (g/L) | 2.913 | 3 |
| Temperature, T (K) | 302.323 | 303 |
| Removal of BG dye (%) | 90.417 | 92.1 |

### 4.2 Interaction Effects of Adsorption Variables

Figures 17(a)–17(f) present response surface plots illustrating interaction effects between pairs of variables on BG removal, with the remaining variables held at their center levels. The curved surfaces confirm the nonlinear nature of the system and the importance of quadratic and interaction terms in describing the response.

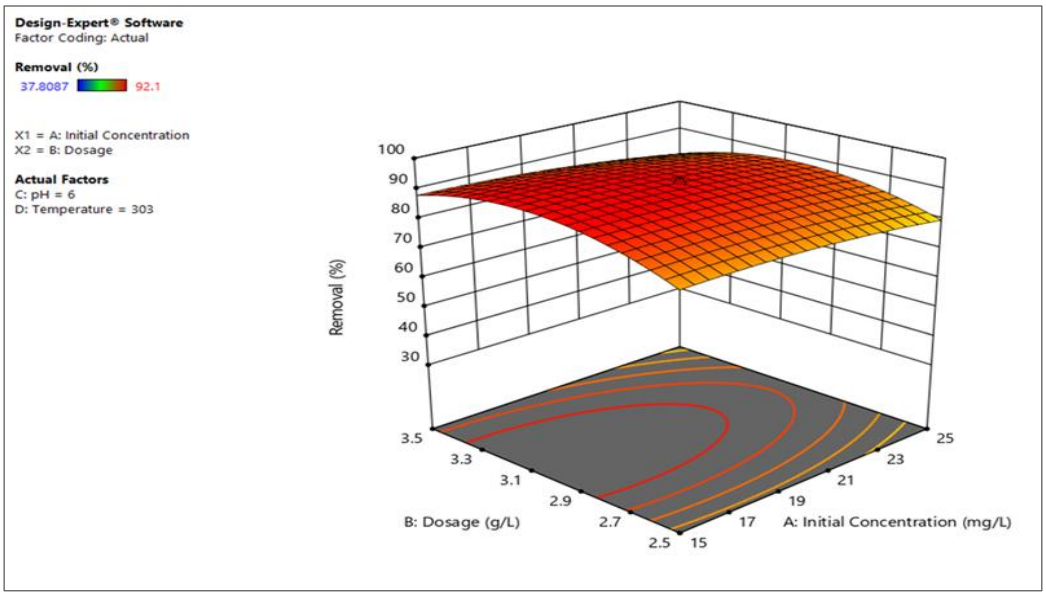


**Figure 17(a).** Response surface plot showing the combined effects of dosage and initial concentration on BG removal (%).

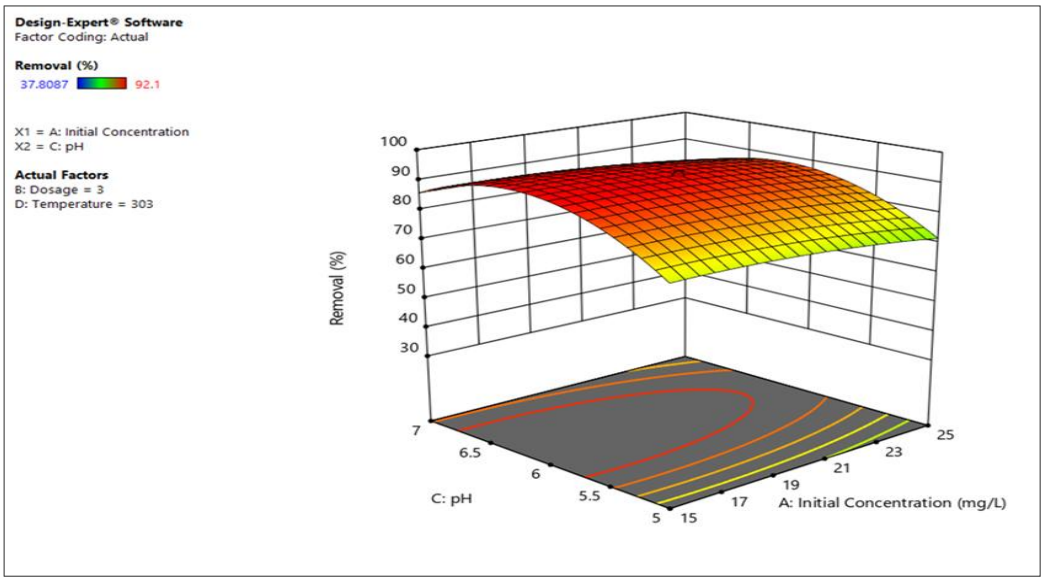


**Figure 17(b).** Response surface plot showing the combined effects of pH and initial concentration on BG removal (%).

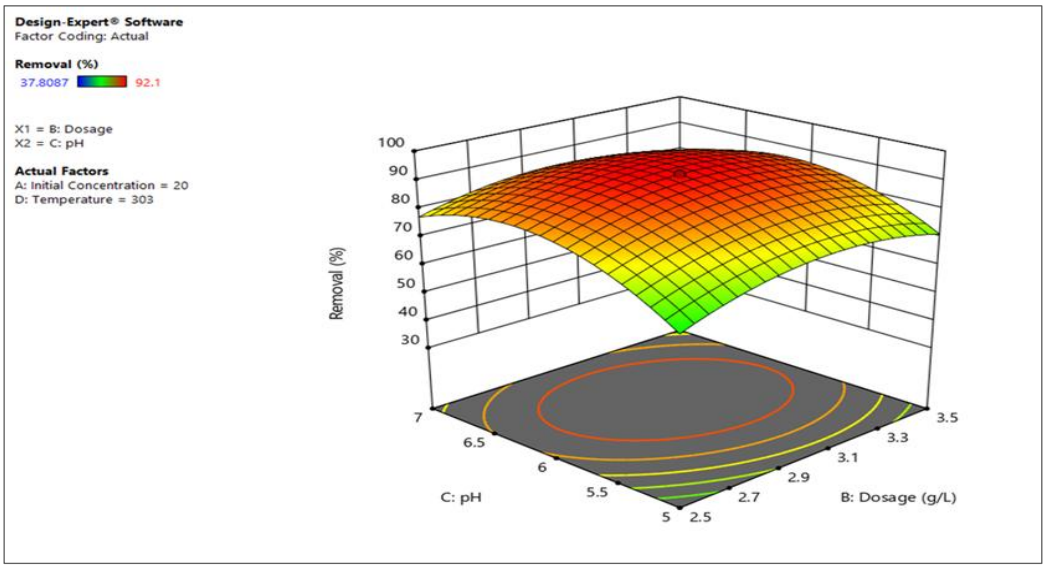


**Figure 17(c).** Response surface plot showing the combined effects of pH and dosage on BG removal (%).

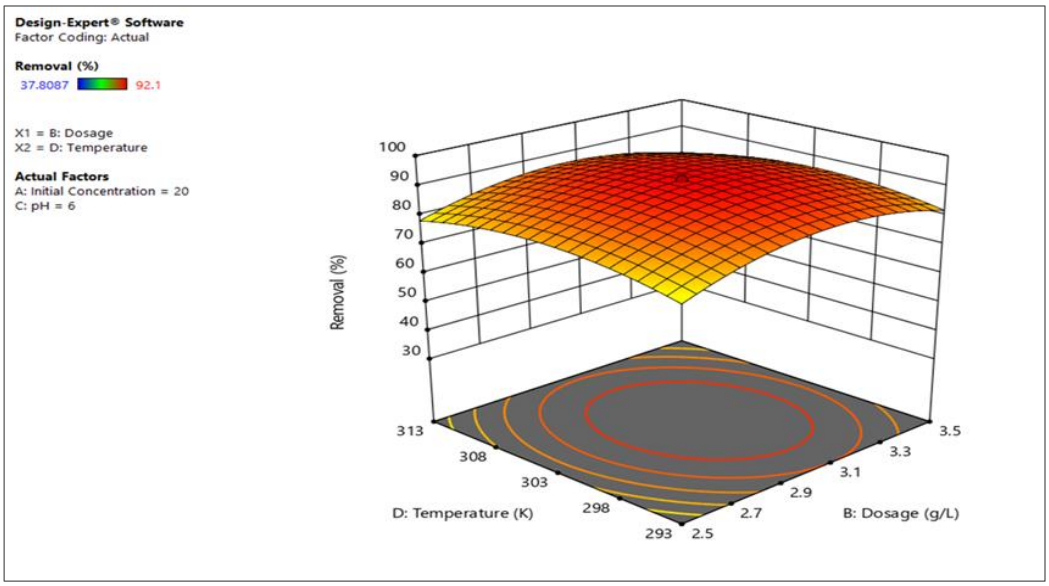


**Figure 17(d).** Response surface plot showing the combined effects of temperature and dosage on BG removal (%).

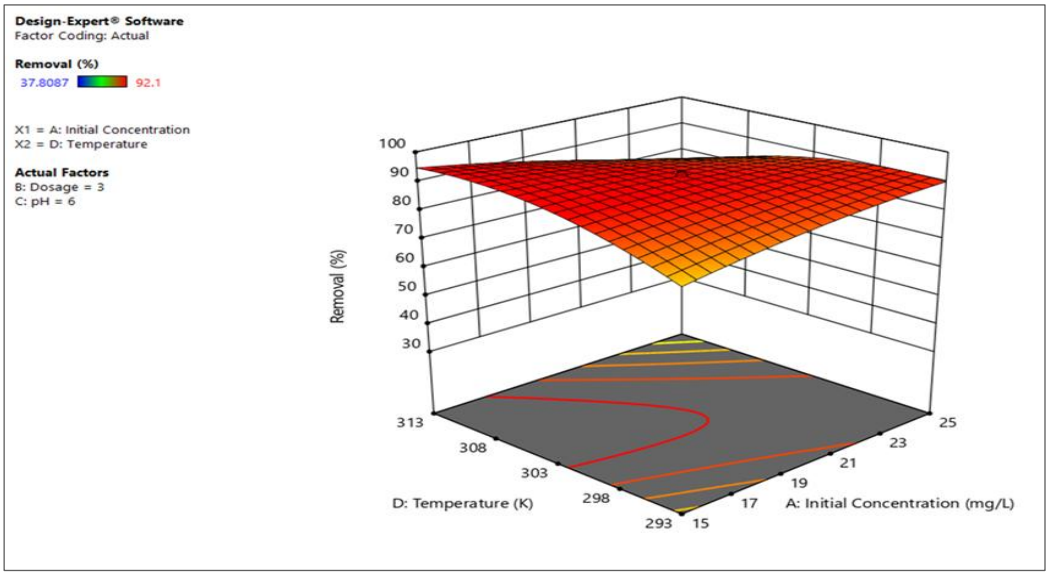


**Figure 17(e).** Response surface plot showing the combined effects of temperature and initial concentration on BG removal (%).

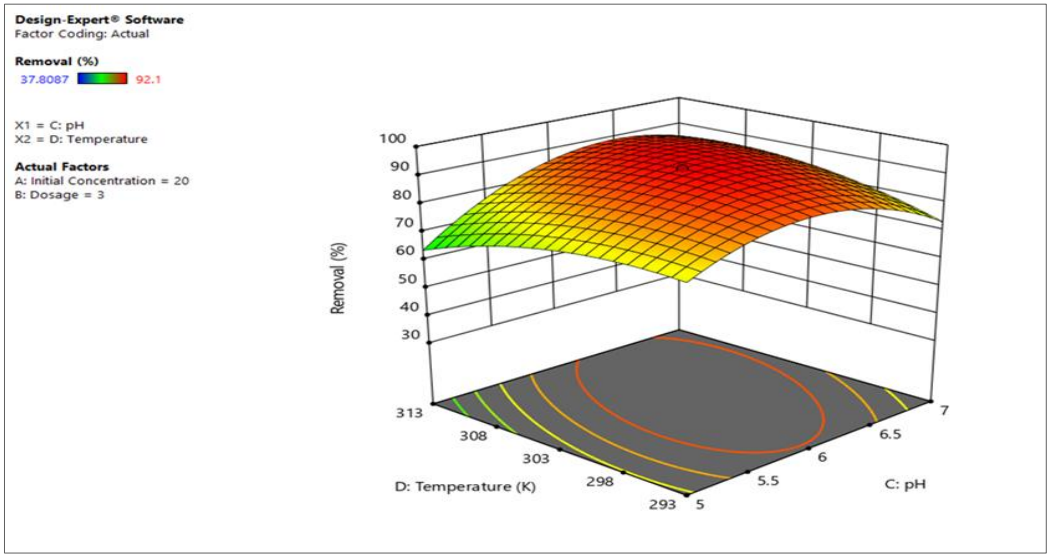


**Figure 17(f).** Response surface plot showing the combined effects of temperature and pH on BG removal (%).

## 5. Conclusion

Co–MgO nanoparticles were synthesized using *Moringa oleifera* leaf extract and applied as an adsorbent for Brilliant Green removal from aqueous solution. The main findings are summarized below:

1) SEM and XRD confirmed the formation of crystalline MgO-based nanostructures with cobalt incorporation; FTIR and EDX supported the presence of Mg–O/Co–O bonds and the expected elemental composition.

2) In batch experiments, BG removal increased with contact time and adsorbent dosage, and an optimum pH of ~6 was observed under the studied conditions.

3) Equilibrium data were best described by the Freundlich isotherm ($R^2$ = 0.998), indicating heterogeneous surface adsorption with non-ideal uptake behavior.

4) Kinetic data were well represented by the pseudo-second-order model ($R^2$ = 0.9994).

5) Thermodynamic parameters ($\Delta H° < 0$ and $\Delta G° < 0$) indicated a spontaneous and exothermic adsorption process.

6) RSM optimization (CCD) identified contact time ≈ 100 min, $C_0$ = 20 mg/L, pH = 6, dosage = 3 g/L, and T = 303 K as favorable conditions, achieving 92.1% BG removal.

## Declarations

**Acknowledgments:** The authors gratefully acknowledge all the individuals who contributed to this paper.
**Artificial Intelligence (AI) Use Statement:** The authors declare that no artificial intelligence (AI) tools or AI-assisted technologies were used in the conceptualization, design, data collection, analysis, interpretation, or writing of this manuscript.
**Author Contributions:** AMM: Implementation of the study protocol, conducted all laboratory experiments, performed data collection, data processing, and statistical analysis, conducted a comprehensive literature review, drafted the original manuscript, prepared figures and tables, and contributed to manuscript writing and revision; CAIR: Supervised the experimental work, provided guidance on methodology, interpreted the results, reviewed and critiqued manuscript drafts, and edited and approved the final manuscript; HNHK: Developed the research concept, refined the study objectives and hypotheses, assisted with the literature survey, contributed to data interpretation, prepared section drafts, and edited and critically revised the manuscript; TLB: Provided support for the research concept, contributed to the literature review, assisted in reviewing and revising the manuscript for intellectual content, and offered constructive critiques and edits; RAM: Contributed to the study design, oversaw project progress, provided guidance on technical aspects of the research, participated in manuscript preparation, and reviewed and approved the final manuscript.
**Conflict of Interest:** The authors declare no conflict of interest.
**Consent to Publish:** The authors consent to the publication of this paper in International Journal of Recent Innovations in Academic Research.
**Data Availability Statement:** The data presented in this study are available from the corresponding author upon reasonable request.
**Funding:** This research received no external funding.
**Institutional Review Board Statement:** Not applicable.
**Informed Consent Statement:** Not applicable.
**Research Content:** The content of this manuscript is original and has not been published elsewhere.

## References

1. Kiran, S., Ashraf, A., Rahmat, M., Afzal, G., Abrar, S. and Asif, S. 2022. Green synthesis of magnesium oxide nanoparticles using leaves of *Iresine herbstii* for remediation of Reactive Brown 9 dye. Global NEST Journal, 24(2): 291–296.
2. Jeena, T., Geetha, M.P., Suchetan, P.A., Ronald, N. and Amrutha, K. 2023. Influence of cobalt doping on chemical and green synthesized magnesium oxide nanoparticles for enhanced photocatalytic evaluation, adsorption studies, antimicrobial analysis and corrosion inhibition study. SSRN Electronic Journal. https://ssrn.com/abstract=4452536
3. Harki, D.A.H., Naghipour, A. and Fardood, S.T. 2024. Eco-friendly synthesis and characterization of $Mg_{0.5}Co_{0.5}Fe_2O_4$ magnetic nanoparticles for photocatalytic degradation of Congo Red dye. Case Studies in Chemical and Environmental Engineering, 10: 101016.

4. Badr, M., Abdelrazek, A.M., Uosif, M.A.M. and Sayyed, M.I. 2023. Structural, morphological, and optical characterization of MgO nanoparticles synthesized by sol–gel method for photocatalytic and antibacterial applications. Journal of Sol-Gel Science and Technology, 107(1): 186–196.
5. Arunachalam, V., Muthukumaran, V., Kaid, M.K.A., Bakkiyaraj, D.K., Rathinavel, K. and Abdelgawad, M.I.A. 2022. Plant-mediated green synthesis of magnesium oxide nanoparticles for the removal of Congo Red dye and its antibacterial applications. Environmental Research, 215(Part 4): 114387.
6. Drummer, S., Mkhari, O. and Chowdhury, M. 2024. Green synthesis of $Co_3O_4$ nanoparticles using spent coffee: Application in catalytic and photocatalytic dye degradation. Next Nanotechnology, 6: 100069.
7. Rashid, S., Islam, S., Qamer, S., Ali, M., Fatima, M., Javaid, L., Ali, A., Sarwar, A. and Farooq, A.S. 2025. A review of green synthesized magnesium oxide nanoparticles coated textiles. Journal of Industrial Textiles, 55: 1–48.
8. Enache, A.C., Cojocaru, C., Samoila, P., Ciornea, V., Apolzan, R., Predeanu, G. and Harabagiu, V. 2023. Adsorption of Brilliant Green dye onto a mercerized biosorbent: Kinetic, thermodynamic, and molecular docking studies. Molecules, 28: 4129.
9. Alkaim, A.F., Mahdi, A.B., Altimari, U.S., Al Qaysi, S., Ramadan, M.F. and Aljeboree, A.M. 2023. Removal of Brilliant-Green dye using carbon-loaded zinc oxide nanoparticles: A comparative isotherm study. Engineering Proceedings, 59: 59152.
10. Venkatachalam, M., Krishnamoorthy, S., Alagarsamy, D. and Devanesan, R. 2021. *Moringa oleifera* leaf extract–mediated green synthesis of ZnO nanoparticles: Characterization and their antibacterial activity. Journal of Chemistry, 2021: 1–10.
11. Ragab, A., Ahmed, I. and Bader, D. 2019. The removal of Brilliant Green dye from aqueous solution using nano hydroxyapatite/chitosan composite as a sorbent. Molecules, 24(5): 847.
12. Ali, A.F., Kovo, A.S. and Adetunji, S.A. 2017. Methylene Blue and Brilliant Green dyes removal from aqueous solution using agricultural wastes activated carbon. Journal of Encapsulation and Adsorption Sciences, 7: 95–107.
13. Saxone, V.A., Sonde, O.I., Oladoyinbo, F.O., Afolabi, T.A., Adetunji, O., Adsokan, H.A. and Dare, E.O. 2017, May 18–20. Green synthesis, characterisation and optical properties of silver–cobalt nanohybrid. In: Proceedings of the Chemical Society of Nigeria (CSN) 2nd Zonal International Conference, Exhibition and Workshop, South West (pp. 38–40). Moshood Abiola Polytechnic, Abeokuta, Ogun State, Nigeria.
14. Hafeez, M., Shaheen, R., Akram, B., Zain-ul-Abdin, Haq, S., Mahsud, S., Ali, S. and Khan, R.T. 2020. Green synthesis of cobalt oxide nanoparticles for potential biological applications. Materials Research Express, 7: 025019.
15. Taghavi Fardood, S., Forootan, R., Moradnia, F., Afshari, Z. and Ramazani, A. 2020. Green synthesis, characterization, and photocatalytic activity of cobalt chromite spinel nanoparticles. Materials Research Express, 7: 015086.
16. Kothari, R., Sen, S. and Rai, S. 2022. Green synthesis of cobalt sulphide nanoparticles using synthesised cobalt (II) complex as a single route intermediate. Digest Journal of Nanomaterials and Biostructures, 17(2): 403–420.
17. Vinayak, V., Khirade, P.P., Birajdar, S.D., Gaikwad, P.K., Shinde, N.D. and Jadhav, K.M. 2015. Low temperature synthesis of magnesium doped cobalt ferrite nanoparticles and their structural properties. International Advanced Research Journal in Science, Engineering and Technology, 2(3): 55–58.
18. Nasrin, F., Hossen, M.K., Bhuiyan, M.R.A.H. and Rahman, M.S. 2020. Synthesis and characterization of pure and cobalt doped zinc oxide nanoparticles. American Journal of Nanosciences, 6(1): 1–7.
19. Khan, A., Ahmed, S., Mahmood, F. and Khokhar, M.Y. 2003. A novel dye-doped sol–gel silica sorbent for the removal of cobalt. Adsorption Science and Technology, 21(3): 205–215.
20. Rajadurai, L., Sambasivam, R., Dash, C.S., Ramalingam, R.J., Dhiwahar, A.T., Al-lohedan, H., Vidhya, J. and Sundararajan, M. 2024. Effective removal of tetracycline hydrochloride under visible light using cobalt doped magnesium ferrite nanoparticles. Research Square. https://doi.org/10.21203/RS.3.RS-4006784/V1
21. Sánchez-Sánchez, Á., Suárez-García, F., Martínez-Alonso, A. and Tascón, J.M.D. 2015. Synthesis, characterization and dye removal capacities of N-doped mesoporous carbons. Journal of Colloid and Interface Science, 450: 91–100.

22. Prasanth, R., Dinesh Kumar, S., Jayalakshmi, A., Singaravelu, G., Govindaraju, K. and Ganesh Kumar, V. 2019. Green synthesis of magnesium oxide nanoparticles and their antibacterial activity. Indian Journal of Geo-Marine Sciences, 48(8): 1210–1215.

23. Labuschagné, F.J.W.J., Wiid, A., Venter, H.P., Gevers, B.R. and Leuteritz, A. 2018. Green synthesis of hydrotalcite from untreated magnesium oxide and aluminum hydroxide. Green Chemistry Letters and Reviews, 11(1): 18–28.

24. Sunder, A. and Pai, K.S.R. 2017. Green synthesis of veratraldehyde using immobilized fungal laccase. ChemistrySelect, 2(18): 5269–5276.

25. Heussien, Z., Yousef, N., Temark, H. and Ebnawaled, A.A. 2025. Green magnesium oxide nanoparticles (MgO-NPs) as an antibacterial agent against multidrug-resistant bacteria causing tonsillitis. AUN Journal of Applied Sciences, 3(1): 53–76.

26. Younis, S., Ijaz, I., Nazir, A., Bukhari, A., Rizwan, A. and Gilani, E. 2020. Synthesis, characterization and bacterial evaluation of cobalt nanoparticles using drumstick leaf extract via green route (EasyChair Preprint No. 2386). EasyChair.

27. Elhalil, A., El Haimouti, H., Fekhaoui, M. and Abouarnadasse, M. 2021. Green synthesis of Ca/MgO nanosorbent for the treatment of wastewater containing toxic dyes. Environmental Nanotechnology, Monitoring and Management, 15: 100433.

28. Rao, S.V.D.S., Preetha, S., Sekar, S., Ryntathiang, I., Behera, A., Saravanan, S. and Jothinathan, M.K.D. 2024. Green synthesis and characterization of cobalt nanoparticles using *Butea monosperma* flower extract and their biocompatibility studies. Texila International Journal of Public Health, 12(3): 1-18.

29. Coşkun, Y.İ., Aksuner, N. and Yanik, J. 2019. Sandpaper wastes as adsorbent for the removal of Brilliant Green and Malachite Green dye. Acta Chimica Slovenica, 66: 402–413.

30. Yadav, M., Arya, S. and Kumar, S. 2022. Multifunctional copolymers for Brilliant Green dye removal: Synthesis, characterization and photocatalytic degradation studies. Polymer Bulletin, 79: 2881–2903.

31. Singh, A., Srivastava, A., Tripathi, A. and Dutt, N.N. 2016. Optimization of Brilliant Green dye removal efficiency by electrocoagulation using response surface methodology. World Journal of Environmental Engineering, 4(2): 23–29.

32. Crini, G. 2006. Non-conventional low-cost adsorbents for dye removal. Bioresource Technology, 97: 1061–1085.

33. Foo, K.Y. and Hameed, B.H. 2010. Insights into the modeling of adsorption isotherm systems. Chemical Engineering Journal, 156: 2–10.

34. Ho, Y.S. and McKay, G. 1999. Pseudo-second order model for sorption processes. Process Biochemistry, 34: 451–465.

35. Robinson, T., McMullan, G., Marchant, R. and Nigam, P. 2001. Remediation of dyes in textile effluent: A critical review. Bioresource Technology, 77: 247–255.

36. Crini, G. and Badot, P.M. 2008. Application of chitosan, a natural aminopolysaccharide, for dye removal from aqueous solutions. Progress in Polymer Science, 33: 399–447.

37. Gupta, V.K. and Suhas. 2009. Application of low-cost adsorbents for dye removal – A review. Journal of Environmental Management, 90: 2313–2342.

38. Ayawei, N., Ebelegi, A.N. and Wankasi, D. 2017. Modelling and interpretation of adsorption isotherms. Journal of Chemistry, 2017: 1–11.

39. Langmuir, I. 1918. The adsorption of gases on plane surfaces of glass, mica and platinum. Journal of the American Chemical Society, 40: 1361–1403.

40. Myers, R.H., Montgomery, D.C. and Anderson-Cook, C.M. 2016. Response surface methodology: Process and product optimization using designed experiments (4th ed.). John Wiley and Sons.

41. Singh, A., Srivastava, A., Tripathi, A. and Dutt, N.N. 2016. Optimization of Brilliant Green dye removal efficiency by electrocoagulation using response surface methodology. World Journal of Environmental Engineering, 4(2): 23–29.

42. Box, G.E.P. and Wilson, K.B. 1951. On the experimental attainment of optimum conditions. Journal of the Royal Statistical Society: Series B (Methodological), 13(1): 1–45.

**Citation:** Andriamampandry Mazoa Methode, Ch. Asha Immanuel Raju, Heriniaina Ny Hafaliana Koloina, Tamirat Lamaro Bate and Randrianoelivony Andriniaina Mahefa. 2026. Green-Synthesized Cobalt-Doped Magnesium Oxide Nanoparticles for Efficient Removal of Brilliant Green Dye: Adsorption Study and Process Optimization Using Response Surface Methodology. International Journal of Recent Innovations in Academic Research, 10(1): 86-104.